ICASE REPORT

DOWNSTREAM BOUNDARY CONDITIONS FOR

VISCOUS FLOW PROBLEMS

George J. Fix

Max D. Gunzburger

DOWNSTREAM BOUNDARY CONDITIONS FOR

VISCOUS FLOW PROBLEMS

George Fix

Department of Mathematics, Carnegie-Mellon University
Pittsburgh, Pennsylvania 15213

and

Max D. Gunzburger
Institute for Computer Applications in Science and Engineering
Hampton, Virginia 23665

The problem of the specification of artifical outflow conditions in flow problems is studied. It is shown that for transport type equations incorrect outflow conditions will adversely affect the solution only in a small region near the outflow boundary, while for elliptic equations, e.g., those governing the streamfunction or pressure, a correct boundary specification is essential. In addition, integral outflow boundary conditions for fluid dynamical problems are considered. It is shown that such conditions are well posed, and their effect on the solutions of the Navier-Stokes equations is also considered.

I. Introduction

The selection of appropriate boundary conditions to use on outflow
regions has been a classical problem in computational fluid dynamics.
Normally, the outflow boundaries are artificial in the sense that they are
arbitrarily supplied so that the physical problem can be defined in a
bounded region. A typical situation is given in Figure 1, and represents
a flow in an expanding channel. The inflow conditions in effect define
the problem. Thus along AG in Figure 1 we specify u and v which are
the x and y components of the velocity field. Along a solid wall
such as AC the correct boundary conditions are that there is no flow
through the wall, i.e., v = 0, and with viscous forces present, that
there is no flow tangent to the wall, i.e., u = 0. The problem arises
at the outflow CD. This line was added in order to make the computational
domain, Ω, finite, and since it occurs in the fluid itself, correct
boundary conditions along this line are by no means clear either mathemati-
cally or physically.

It is not surprising that the literature of the downstream boundary con-
dition problem is apparently contradictory. For example, Cheng [1], reported
numerical experiments that indicated that for transport type equations, al-
most anything could be specified provided that the outflow boundary (such as
BC in Figure 1) was far enough downstream, i.e., away from corner points such
as E. On the other hand Roache [2] specifically suggests the use of down-
stream continuation which in effect sets second derivatives equal to zero
on the outflow BC.

In this paper we show that if the problem is formulated in terms of the
streamfunction ψ and the vorticity ζ

$$\frac{\partial \zeta}{\partial t} + \frac{\partial \psi}{\partial y}\frac{\partial \zeta}{\partial x} - \frac{\partial \psi}{\partial x}\frac{\partial \zeta}{\partial y} = \frac{1}{R}\Delta\zeta \qquad (1.1)$$

$$\Delta\psi = \zeta \qquad (1.2)$$

then any specification of vorticity on the outflow yields sufficiently accurate solutions of Eq. (1.1) independent of the downstream position of the outflow boundary. Indeed, a change in the outflow specification of the vorticity will affect the solution only in a small boundary layer near the outflow. This is verified in Section II for one dimensional problems and in Section III for two dimensional problems. In addition, it is verified for a representative difference scheme.

On the other hand the situation is entirely different for the elliptic equation (1.2). Differences in outflow specification significally propagate into the interior and therefore it is crucial that the correct outflow condition on the streamfunction be specified. Thus as the outflow is moved far downstream it is known that indeed $\partial^2\psi/\partial x^2$ approaches zero on the outflow, or alternately, since one knows the flow at large distances from E, one could just as well specify ψ or $\partial\psi/\partial x$ along CD. However, if the outflow is moved in or if one is dealing with problems where there are no known asymptotic downstream solutions, specification of these quantities will yield spurious solutions.

In many problems of the latter type integral conditions on the flow can be accurately estimated. For example, in limited region ocean circulation problems, mass flows, i.e., volume integrals of the flow, can be measured [3]. In this paper we consider, apparently for the first time, integral boundary conditions for Eqs. (1.1) and (1.2). Conditions of this type are included in the work presented in Section II and III. Moreoever, in Section IV we indicate that such problems are well posed and that a representative finite difference scheme is not adversely affected by the integral boundary conditions.

II. A Simple 1-D Example for the Transport Equation

We wish to study the effects due to the specification of outflow conditions on a transport equation such as Eq. (1.1). To illustrate the main ideas we begin with the linear equation

$$\frac{\partial w}{\partial t} + \frac{\partial w}{\partial x} = \frac{1}{R} \frac{\partial^2 w}{\partial x^2} \quad , \quad 0 < x < 1. \tag{2.1}$$

At the inflow, $x = 0$, we specify

$$w(0,t) = w_{in}(t). \tag{2.2}$$

Three alternatives will be considered for outflow boundary conditions, two of which are in common use. The first condition, hereafter Option A, is to specify

$$w(1,t) = w_{out}(t). \tag{2.3}$$

The second, commonly called downstream continuation and in this paper denoted as Option B, is

$$\partial^2 w/\partial x^2 (1,t) = 0. \tag{2.4}$$

Option C is the integral condition

$$\int_0^1 w(x,t)dx = m(t). \tag{2.5}$$

Other outflow conditions, such as specifying the first derivative, could also be considered. Their effects could be deduced in a smilar manner to the following development for Options A, B, and C.

The disadvantages of Options A and C are that one does not usually know w_{out} and m. The disadvantage of Option B is that it may not be consistent with the type of flow that is being modeled. There is also the mathematical

problem involved with the specification of higher order derivatives on the boundary. We assert, nevertheless, that in each case the errors in the solution of Eq. (2.1) are restricted to an outflow boundary layer.

Before proving these assertions, let us consider discrete analogs for Eqs. (2.1) - (2.5). To keep the analysis simple, we choose the simple explicit finite difference approximation to Eq. (2.1)

$$(w_j^{n+1} - w_j^n)/\tau + (w_{j+1}^n - w_{j-1}^n)/2h = (w_{j+1}^n - 2w_j^n + w_{j-1}^n)/Rh^2 \qquad (2.6)$$

for $1 < j \leq J - 1$ and $n \geq 0$, where $J = 1/h$, h and τ are the uniform grid sizes in x and t, respectively, and $w_j^n \approx w(jh, n\tau)$. The three boundary conditions in addition to the inflow condition

$$w_o^n = w_{in}(n\tau) \qquad (2.7)$$

are

$$\text{A:} \qquad w_J^n = w_{out}(n\tau) \qquad (2.8)$$

$$\text{B:} \qquad w_J^n - 2w_{J-1}^n + w_{J-2}^n = 0 \qquad (2.9)$$

and

$$\text{C:} \qquad h \sum_{j=0}^{J-1} \left[w_j^n + w_{j+1}^n \right] = 2m(n\tau) \qquad (2.10)$$

The last equation is obtained from Eq. (2.5) via trapezoidal quadratures.

Before analyzing Eqs. (2.1) - (2.5) and Eqs. (2.6) - (2.10), we report some numerical experiments. First we consider the problem whose exact solution is known, namely

$$W(x,t) = \sin(ax - at) \exp(-a^2 t/R).$$

Then, for our computations we take the inflow and initial conditions to be $W(0,n\tau)$ and $W(jh,0)$, respectively. We arbitrarily specify $w_{out} = m = 0$ so that all three outflow conditions are in error. Figures 2 and 3 show the pointwise error resulting from the computations, i.e.

$$E_j^n = w_j^n - W(jh,n\tau)$$

as a function of x for different values of t. The parameters used are $J = 50$, $\tau = .001$, $a = 4.5\pi$, $R = 10$ for Figure 2 and $R = 20$ for Figure 3. The initial condition on W is also shown in order to provide a reference scale. Note that for all three options, $E_j^n \approx 0$ for a large part of the domain $0 \leq x \leq 1$ and that $E_j^n \neq 0$ only near the outflow boundary. The thickness of the region in which errors occur is essentially the same for all three options. Furthermore, for $R = 20$, the thickness of the boundary layer is smaller than for $R = 10$. This is especially evident for Option C, where the boundary layer is quite pronounced. In fact, from tabular data, it can be shown for all three options that the boundary layer thickness δ obeys the empirical relation

$$\delta \sim 1/R \tag{2.11}$$

where $\delta = 1-x_B$ and x_B is the smallest value of x at which the error is a given small percentage of the maximum error along a particular curve. The relation (2.11) is largely independent of the choice of the "given small percentage."

We next turn to an example, again for Eq. (2.1), whose transient solution is not known, but for which the graph of the solution is simple enough so that the transient can be easily followed. We consider

$$w(x,0) = b \exp\{-(x-c)^2/d^2\} \quad \text{and} \quad w(0,t) = 0$$

to be the initial and inflow conditions, respectively. Then the steady state solution of Eq. (2.1) in the semi-infinite domain $0 \le x \le \infty$ is zero. We take as outflow conditions

$$w_{out} = A \ , \quad \partial^2 w/\partial x^2 \big|_{x=1} = B \quad \text{and} \quad m = C \qquad (2.12)$$

so that all three outflow conditions are in error, even in the steady state. A, B, and C are interpreted as being errors in the specification of the corresponding outflow condition. Figure 4 shows w as a function of x for different values of t with $J = 50$, $\tau = .0025$, $b = 10$, $c = .8$, $d = .05$, and $A = B = C = 1$. The steady state solution fails to vanish only in a region near the outflow boundary regardless of the option chosen so that again, errors due to the incorrect specification of outflow conditions are trapped in a boundary layer near the outflow. Experiments at different Reynolds' numbers confirm the reciprocal relation (2.11). For Figure 5, the computations of Figure 4 are repeated for $A = B = C = 0$, so that the outflow conditions are correct for the steady state but not for the transient solution. The correct steady state is now achieved for all x for all three options. Furthermore, comparing Figures 4 and 5, we see that except for a small region near the outflow, all six transient solutions are in good agreement. This indicates that away from the outflow boundary, the transient solution is correctly computed not only regardless of which option is chosen, but independent of the actual numerical values of A, B, and C chosen in Eq. (2.12).

Many other experiments were performed, both on Eq. (2.1) and on nonlinear equations such as Burgers' equation. In all cases the boundary layer phenomena reported above was reproduced, and therefore it seems that this behavior is unaffected by the nonlinearities of the differential equation or by complications on the inflow and initial conditions.

We now turn to the analysis of the continuous equation (2.1) and of its discrete approximation Eq. (2.6). Table I lists the exact steady state solution of Eq. (2.1) with $w_{in} = 0$ and outflow conditions given by Eq. (2.12). Also shown is the behavior of w for different values of $\varepsilon = 1-x$ and R. Note that away from $x = 1$, all solutions decay exponentially. Since the solution of the steady state problem without the artificial outflow boundary is identically zero, we see that introducing the artificial boundary causes an error only near $x = 1$. In fact, using our definition of boundary layer thickness we see that $\delta \approx -\ln\sigma/R$ where σ is the "given small percentage." This verifies the experimental result Eq. (2.11).

Referring to Table I, Option B seems to have the advantage of the factor $1/R^2$ in the erroneous boundary layer solution. However, experience shows that errors in the second derivative specification, i.e. B, can often be large, especially when finite disturbances are advecting out of the region at the outflow. Therefore, the advantage of the $1/R^2$ factor may be lost due to the largeness of B. On the other hand, Option C seems to have the disadvantage of having a solution proportional to R in the boundary layer. However, due to the exponential decay factor, this does not appreciably affect the solution outside the boundary layer. In fact, at larger Reynolds' number, this "large" solution may help identify the boundary layer.

Table II lists the exact steady state solution of Eq. (2.6) and the asymptotic rates of convergence (as $R_c = Rh/2 \to 0$) to the continuous solution. Note that all three options yield discrete solutions which converge to the corresponding continuous solution. Therefore as $R_c \to 0$, the discrete solutions exhibit the same boundary layer behavior as the continous solutions. Options B has a slower rate of convergence because of the one sided difference used in Eq. (2.9).

Although the above results are for the steady state, a simple perturbation analysis of the unsteady equations show that similar results also hold for the transient solution. Furthermore, we emphasize that the appearance of the boundary layer phenomena near the outflow is in no way tied to the particular choice of discrete approximation used above, e.g. Eq. (2.6). This approximation was chosen solely for its simplicity.

III. A 2-D Example for the Navier-Stokes Equations

In this section we present computational results for the vorticity and streamfunction in the channel depicted in Figure 1. Three options for the outflow conditions are considered. Options B and C are analogous to those in Section II, while for the sake of variety, Option A of that section is replaced by Option A', a specification of first derivatives. Eqs. (1.1) and (1.2) are discretized by the use of the simple explicit finite difference scheme in which time derivatives are approximated by a forward difference quotient, i.e.,

$$\partial \zeta(t_n, x_i, y_j)/\partial t \approx (\zeta_{i,j}^{n+1} - \zeta_{i,j}^n)/\tau$$

and space derivatives are approximated by centered difference quotients, e.g.,

$$\partial^2 \psi(t_n, x_i, y_j)/\partial y^2 \approx (\psi_{i,j+1}^n - 2\psi_{i,j}^n + \psi_{i,j-1}^n)/k^2$$

and

$$\partial \zeta(t_n, x_i, y_j)/\partial x \approx (\zeta_{i+1,j}^n - \zeta_{i-1,j}^n)/2h$$

where

$$\zeta_{i,j}^n \approx \zeta(t_n, x_i, y_j) \quad , \quad \psi_{i,j}^n \approx \psi(t_n, x_i, y_j)$$

-8-

and τ, h and k are the step sizes in t, x, and y, respectively. At the inflow boundary (AG in Figure 1) the flow is assumed to be a fully developed Poiseuille flow so that [4]

$$\psi_{in} = 4Ud(y/d)^2(1/2 - y/3d) \quad \text{and} \quad \zeta_{in} = (4U/d)(1 - 2y/d) \quad (3.1)$$

where d is the distance AG and U is the maximum velocity of the Poisseuille profile. Consistent with Eq. (3.1), along the upper and lower walls the streamfunction is given by

$$\psi_{low} = 0 \quad \text{and} \quad \psi_{up} = 2Ud/3$$

respectively. The wall vorticities are calculated using the Thom formula [2], e.g., along the wall AC

$$\zeta_{i,j}^n = 2(\psi_{i,j}^n - \psi_{i,j-1}^n)/h^2.$$

The initial conditions are $\zeta(t=0) = \psi(t=0) = 0$ and our aim is to compute the steady state solutions for ζ and ψ. The fixed parameters used in computing the results discussed below are R = 20, h = k = 1/16, τ = 1/400, d = 1/2, the distance GE = 1/2, and the distance CD = 1.

In order to complete the specification of the problem we must fix the position of the outflow CD, i.e., choose the distance ED, and then specify outflow conditions on both ζ and ψ. For two of these we choose the specification of the first derivative

$$A': \quad h(\partial\psi/\partial x)|_{CD} = \psi_{I,j}^n - \psi_{I-1,j}^n \quad (3.2)$$

the specification of the second derivative

$$B: \quad h^2(\partial^2\psi/\partial x^2)|_{CD} = \psi_{I,j}^n - 2\psi_{I-1,j}^n + \psi_{I-2,j}^n \quad (3.3)$$

and likewise for ζ, where I is the index corresponding to the line CD.
For Option C we could approximate the integral

$$I_\psi(t,y) = \int_d^y dy \int_{x_L}^{x_R} dx\,\psi(t,x,y)$$

and similarly for I_ζ, where x_R and x_L are respectively the coordinates
of the line CD and of some vertical line to the left of CD. However,
approximating these integrals would destroy the compact nature of the
approximating scheme since, for instance, any point on the line CD would
be coupled to all the points whose y coordinate is smaller. This coupling
can be alleviated in two ways, and we use one on I_ψ and the other on I_ζ.
Therefore, we impose the outflow conditions

$$I'_\psi = \partial I_\psi/\partial y \quad \text{and} \quad \Delta I_\zeta = I_\zeta(t,y) - I_\zeta(t,y-k) \tag{3.4}$$

which can be approximated by

$$C: \quad I'_\psi(n\tau,jk) = \frac{h}{2}\left(\psi^n_{I-p,j} + 2\sum_{i=I-p+1}^{I-1} \psi^n_{i,j} + \psi^n_{I,j}\right) \tag{3.5a}$$

and

$$\Delta I_\zeta(n\tau,jk) = \frac{hk}{4}\sum_{i=I-p+1}^{I}\left(\zeta^n_{i,j} + \zeta^n_{i-1,j} + \zeta^n_{i-1,j-1} + \zeta^n_{i,j-1}\right) \tag{3.5b}$$

when x_L and x_R are chosen so that $x_R - x_L = ph$. The choice for I'_ψ is
particularly important because it preserves the bandwidth of the matrix
appearing in the discrete approximation to Eq. (1.2).

   We first choose to place the outflow boundary CD "far" downstream,
e.g. ED = 4d = 2, and we then assume that at this position the flow has
settled into a fully developed Poiseuille flow in a channel of width 2d.
Then the left hand sides of Eqs. (3.2), (3.3), and (3.5) may be computed

analytically by using Eq. (3.1) with (y/d) replaced by (y+d)/2d. Computational results show that the solutions due to the three options for the outflow condition are identical in the sense that their pointwise differences (suitably scaled by average values of the variables) are uniformly less than 10^{-4}, which is considerably less than the discretization error of the finite difference scheme. These results are not surprising since we have imposed accurate outflow conditions on both ψ and ζ. This calculation was performed in order to provide a benchmark for the computations reported below.

We now move the outflow boundary CD "close" to the corner point F by choosing ED = d = 1/2 (or x_{CD} = 1). We use the results of the above "exact" calculation to evaluate the left hand sides of the outflow conditions Eqs. (3.2), (3.3), and (3.5). The computational results for all three options are again indistinguishable from each other and from the above "exact" calculation. This shows that for any type outflow condition, including integral conditions, a correct specification will yield correct solutions even when the outflow is in a region of significant flow changes.

With the outflow still at x = 1, we next purposely choose incorrect outflow conditions for both ψ and ζ by choosing the left hand side of all outflow conditions to be zero. The results were poor for all three options. Typical pointwise differences (again suitably scaled) between these calculations and the "exact" ones described above were of the order of 10^{-1} to 10^{-2}. These results, denoted below as being "incorrect," indicate that if the outflow conditions are incorrectly specified, then the solution will be adversely affected everywhere.

We now examine the effect of imposing correct outflow conditions on ψ and incorrect ones on ζ. This is of interest because it is in general much easier to obtain information on ψ, which depends on integrals of the velocity,

than on ζ, which depends on derivatives of the velocity. We label this calculation "correct-incorrect." In Figure 6 we show $(\psi_I-\psi_E)/\bar{\psi}_E$ and $(\psi_{CI}-\psi_E)/\bar{\psi}_E$ along the line FB of Figure 1 and in Figure 7 we show $(\zeta_I-\zeta_E)/\bar{\zeta}_E$ and $(\zeta_{CI}-\zeta_E)/\bar{\zeta}_E$ along the line HK of Figure 1 where the subscripts I, CI, and E refer to the "incorrect," "correct-incorrect" and "exact" calculations respectively, and the bar indicates the average value of the variable. These results are typical of those throughout the flow field. From both figures we see that by imposing correct outflow conditions on ψ, we can significally improve the solution. The errors of the "correct-incorrect" run are, except near the outflow, typically smaller than $h^2 = 1/256$ which is a liberal estimate for the discretization error. For the "incorrect" run, the errors are considerably larger than h^2. In Figure 7, the boundary layer phenomena described in Section II is not as sharply evident because both the ellipticity of the Poisson equation and the nonlinearity of the equations contribute to the smearing of the boundary layer. However, experiments at different Reynolds' numbers confirm that the boundary layer thickness decreases with increasing Reynolds' number. Also note that for the "correct-incorrect" run that Option C has a large error in the boundary layer, but in the interior it is of the same magnitude as the other options. This type of behavior is similar to that encountered in Section II.

There is no reason why one should use the same type of outflow conditions for the ψ and ζ. One could mix the options, choosing judiciously according to the information available, or in the absence of complete information, experimenting to determine which combination least affects the solution of the specific problem considered.

To summarize, the computational results of this section indicate that an incorrect specification of outflow conditions will result in spurious solutions away from the outflow boundary while a correct specification will result

in a correct solution everywhere regardless of which option for the outflow condition is chosen. Furthermore, the results of Section II extend to two dimensions and to the full Navier-Stokes equations in the sense that if we correctly specify ψ at the outflow, but incorrectly specify ζ, then the errors in the solution are small for large portions of the computational domain and are large only in the vicinity of the outflow boundary. Finally, we have seen that integral outflow conditions on both ζ and ψ are not only implementable, but affect the solution of Eq. (2.1) in much the same manner as commonly used outflow conditions.

IV. Analysis of Integral Conditions for the Poisson Equation

For arbitrary two dimensional domains an attempt to prove that the Poisson equation (1.2) with an integral condition such as Eq. (3.4) imposed on part of the boundary (and Dirichlet data on the rest) constitute a well posed problem would lead us to a complicated analysis involving integral equations. To avoid these complications we consider the model problem

$$\Delta u = f \quad \text{in} \quad \Omega = [0,1] \times [0,1] \tag{4.1}$$

$$u = 0 \quad \text{on} \quad \Gamma_1 \tag{4.2}$$

and

$$\int_0^y dy' \int_\alpha^1 dx u(x,y') = \gamma(y) \quad \text{on} \quad \Gamma_2 = \{(1,y) \,|\, 0 \leq y \leq 1\} \tag{4.3}$$

where α is a fixed number, $0 < \alpha < 1$, and where $\Gamma_1 \cup \Gamma_2 = \Gamma$, the boundary of the region Ω. Figure 8 shows the regions Ω and Ωy, the latter being the domain of integration of the integral appearing in Eq. (4.3). The central idea in our analysis is to solve the Dirichlet problem defined by Eqs. (4.1), (4.2) and

-13-

$$u = \theta(y) \quad \text{on} \quad \Gamma_2 \quad , \tag{4.4}$$

and to choose θ so that Eq. (4.3) is satisfied. To do this we observe that the solution of Eqs. (4.1), (4.2), and (4.4) is

$$u(x,y) = U(x,y|f) + \int_{\Gamma_2} g(x,y|\eta)\theta(\eta)d\eta$$

where

$$U(x,y|f) = \int\int_\Omega G(x,y,\xi,\eta)f(\xi,\eta)d\xi d\eta \quad ,$$

$G(\cdot,\cdot,\cdot,\cdot)$ is the Green's function for the homogeneous problem (Eq. (4.1) plus $u = 0$ on Γ) and g is the normal derivative of G restricted to Γ_2.

We conclude that Eqs. (4.1), (4.2), and (4.3) have a (unique) solution if and only if

$$\gamma_1(y) = \int_{\Gamma_2} \hat{g}(y,\eta)\theta(\eta)d\eta \quad , \quad 0 \leq y \leq 1 \tag{4.5}$$

has a (unique) solution. In Eq. (4.5)

$$\gamma_1(y) = d\gamma/dy - \int_\alpha^1 dxU(x,y|f)$$

and

$$\hat{g}(y,\eta) = \int_\alpha^1 dxg(x,y|\eta).$$

Simple calculations verify that

$$\int_{\Gamma_2} g(x,y|\eta)\theta(\eta)d\eta = \sum_{k=1}^\infty \theta_k \frac{\sinh(k\pi x)}{\sinh(k\pi)} \sin(k\pi y)$$

-14-

where

$$\theta(y) = \sum_{k=1}^{\infty} \theta_k \sin(k\pi y)$$

Thus our integral equation (4.5) becomes

$$\gamma_1(y) = \sum_{k=1}^{\infty} \theta_k \left\{ \frac{\cosh(k\pi) - \cosh(k\pi\alpha)}{k\pi\sinh(k\pi)} \right\} \sin(k\pi y)$$

and thus the unique solvability of Eq. (4.5) is clear.

This calculation also shows that the mean square norm of second derivatives of u is bounded above by the mean square norm of f plus the "5/2 norm" of γ, i.e.,

$$||\gamma||_{5/2} = \left\{ \sum_{k=1}^{\infty} k^5 \gamma_k^2 \right\}^{1/2} \tag{4.6}$$

where

$$\gamma(y) = \sum_{k=1}^{\infty} \gamma_k \sin(k\pi y)$$

This shows that the problem is well posed in the sense that small changes in γ with respect to Eq. (4.6) leads to small changes in u, ∇u and the second derivatives of u in the mean square sense.

Turning to approximations let us consider a uniform grid with nodes at (ih, jh), $0 \leq i,$ $j \leq N = 1/h$. We approximate $u(ih, jh)$ with $u_{i,j}$ where

$$\left[4u_{i,j} - u_{i,j+1} - u_{i,j-1} - u_{i+1,j} - u_{i-1,j} \right] + h^2 f(ih, jh) = 0 \tag{4.7}$$

for $0 < i, j < 1/h$, and with

$$u_{i,j} = 0 \quad \text{for} \quad \begin{cases} i = 0 \ , \quad 0 \le j \le 1/h \\[2ex] 0 \le i \le 1/h \ , \ j = 0 \\[2ex] 0 \le i \le 1/h \ , \ j = 1/h \end{cases} \tag{4.8}$$

At the nodes for which $x = 1$, $0 < y < 1$, we use

$$\frac{h}{2} \sum_{i=i_o}^{\frac{1}{h}-1} \left[u_{i+1,j} + u_{i,j} \right] = \frac{d\gamma}{dy}(jh) = \gamma_1(jh) \tag{4.9}$$

for $0 < j < 1/h$. We assume that $\alpha = (i_o h)$ and without loss of generality we take $f = 0$. The exact solution is thus

$$u(x,y) = \sum_{k=0}^{\infty} \theta_k \frac{\sinh(k\pi x)}{\sinh(k\pi)} \sin(k\pi y) \ . \tag{4.10}$$

A straightforward calculation shows that the solution of the Eqs. (4.7), (4.8), and

$$u_{N,j} = \theta(jh) = \sum_{k=0}^{1/h} \theta_k^h \sin(k\pi jh) \quad , \quad 0 < j < 1/h$$

is given by

$$u_{i,j} = \sum_{k=0}^{1/h} \theta_k^h \left\{ \frac{\sinh(k\pi ih)}{\sinh(k\pi)} \right\} \sin(k\pi jh) + 0(h^2) \tag{4.11}$$

With this representation the unique solvability of Eq. (4.9) is clear once we note that

$$\frac{h}{2} \sum_{i=i_o}^{1/h-1} \left\{ \sinh[k\pi ih] + \sinh[k\pi(i+1)h] \right\} \rightarrow \frac{\cosh(k\pi) - \cosh(k\alpha\pi)}{k\pi}$$

as $h \to 0$. To be sure the difference between the trapezoidal rule quadrature on the left and the exact quadrature on the right is $O(h^2)$, and with this it is easy to see that θ_k^h in Eq. (4.11) differs from θ_k in Eq. (4.10) by $O(h^2)$. An additional calculation gives

$$u(ih,jh) - u_{i,j} = O(h^2) \text{ as } h \to 0 .$$

Therefore the integral boundary condition Eq. (4.3) and its discrete implementation Eq. (4.9) do not adversely affect the accuracy of the finite difference scheme.

REFERENCES

[1] S. I. CHENG, "Numerical Intergration of Navier-Stokes Equations," AIAA J., 8 (1970), 2115-2122.

[2] P. ROACHE, Computational Fluid Dynamics, Hermosa, Albuquerque (1972).

[3] Dynamics and the Analysis of Mode 1, Report of the Mode One Group, MIT Publications, Cambridge (1975).

[4] H. SCHLICHTING, Boundary Layer Theory, McGraw-Hill, New York (1951).

TABLE I.

Solution of the steady state equation $w_x = w_{xx}/R$ with $w(0) = 0$

OPTION	EXACT SOLUTION $w(\epsilon)=w(1-x)=$	BEHAVIOR FOR $\epsilon R \to 0$	BEHAVIOR FOR $\epsilon R = O(1)$	BEHAVIOR FOR $\epsilon = O(1)$
$w(1) = A$	$\dfrac{A\left[e^{-R\epsilon} - e^{-R}\right]}{1 - e^{-R}}$	$A(1-\epsilon R)$	$Ae^{-R\epsilon}$	$O\left(Ae^{-R}\right)$
$w_{xx}(1) = B$	$\dfrac{B\left[e^{-R\epsilon}-e^{-R}\right]}{R^2}$	$\dfrac{B}{R^2}(1-\epsilon R)$	$\dfrac{B}{R^2}e^{-R\epsilon}$	$O\left(\dfrac{B}{R^2}e^{-R}\right)$
$\displaystyle\int_0^1 w(x)dx = C$	$\dfrac{CR\left[e^{-R\epsilon}-e^{-R}\right]}{1-(1+R)e^{-R}}$	$CR(1-\epsilon R)$	$CRe^{-R\epsilon}$	$O\left(CRe^{-R}\right)$

TABLE II.

Solution of steady state difference equations.

$R_c = Rh/2$, $\lambda = (1+R_c)/(1-R_c)$, J = number of intervals.

OPTION	EXACT SOLUTION OF DIFFERENCE EQUATIONS $w_j =$	ASYMPTOTIC ERROR AS $R_c \to 0$ $w_j - w(x_j) =$
A	$\dfrac{A(\lambda^j - 1)}{(\lambda^J - 1)}$	$0\left(R_c^2\right)$
B	$\dfrac{Bh^2\left(\lambda^j - 1\right)}{\cdot\left(\lambda^J - 2\lambda^{J-1} + \lambda^{J-2}\right)}$	$0(R_c)$
C	$\dfrac{C\left(\lambda^j - 1\right)}{h\left\{\dfrac{\lambda^J}{2} + \dfrac{\lambda-\lambda^J}{1-\lambda} - J + \dfrac{1}{2}\right\}}$	$0\left(R_c^2\right)$

Fig. 1. Flow in a channel.
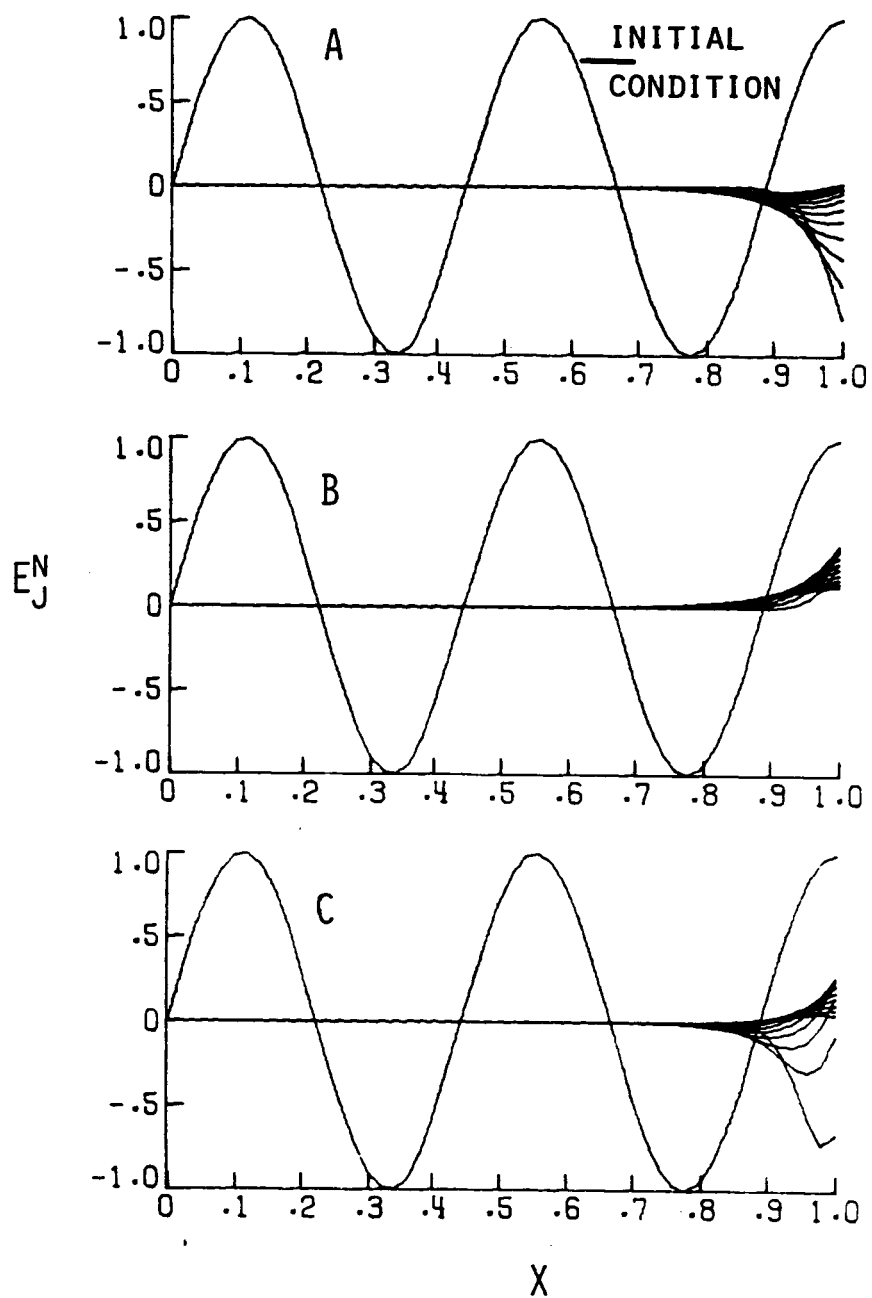
Fig. 2. E_j^n vs. x for R = 10, J = 50, Δt = .001. Plotted every 12Δt.
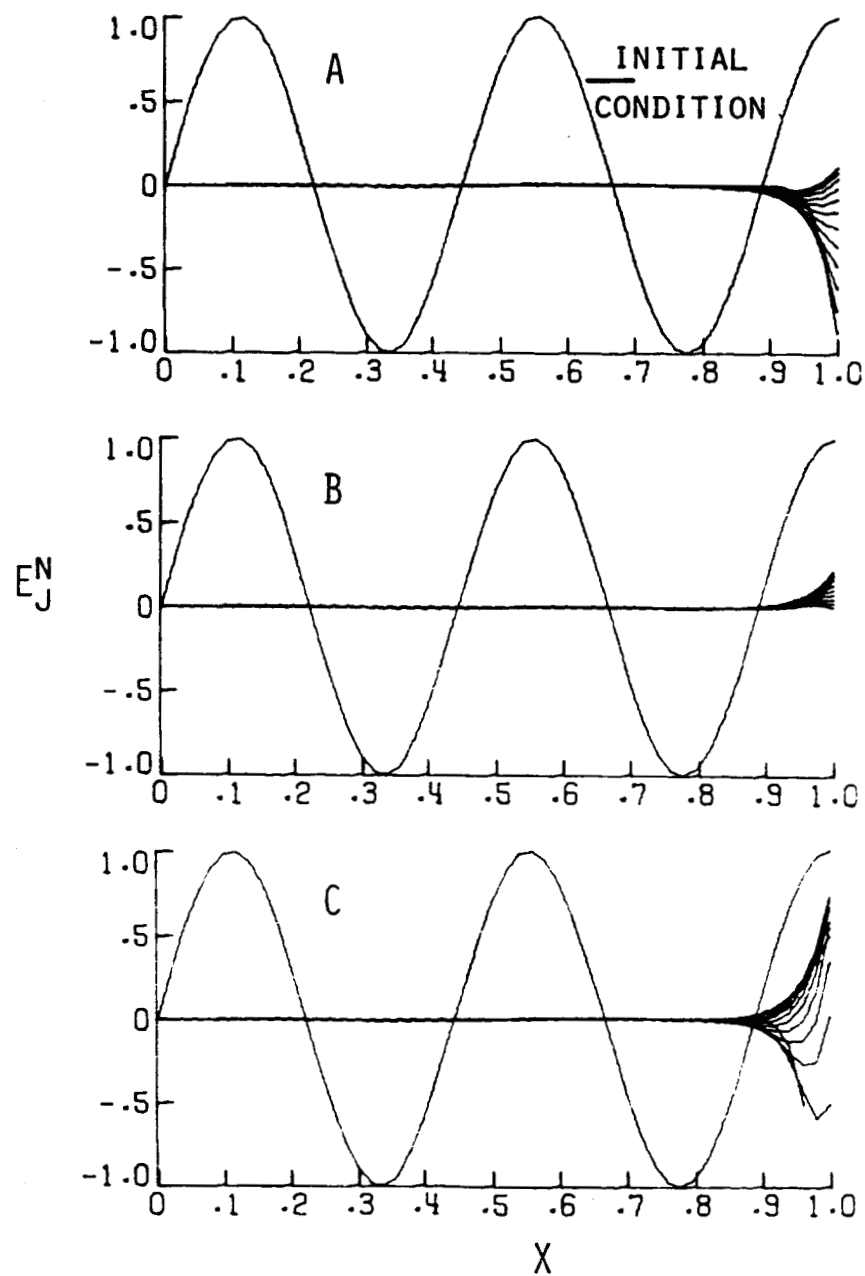
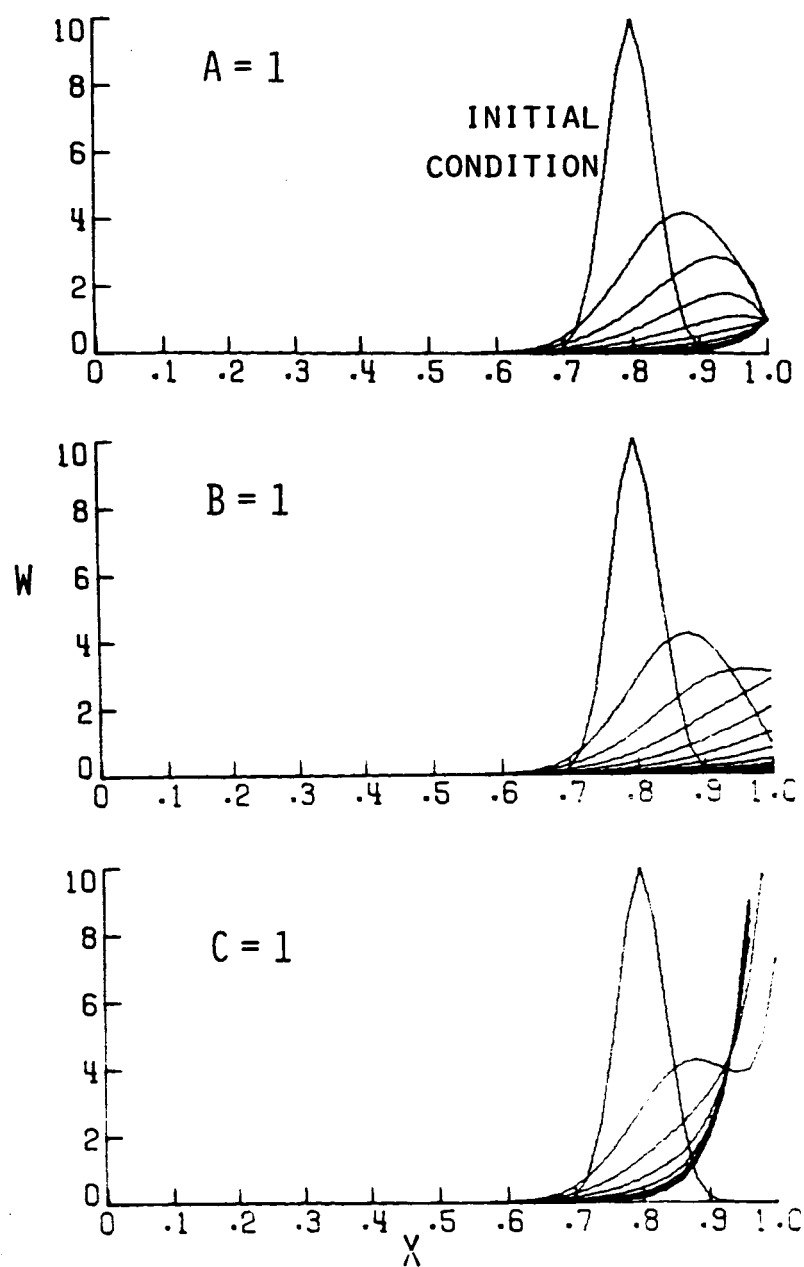Fig. 3. E_j^n vs. x for R = 20, J = 50, Δt = .001. Plotted every 12Δt.

Fig. 4. w vs. x for incorrect steady state outflow conditions.
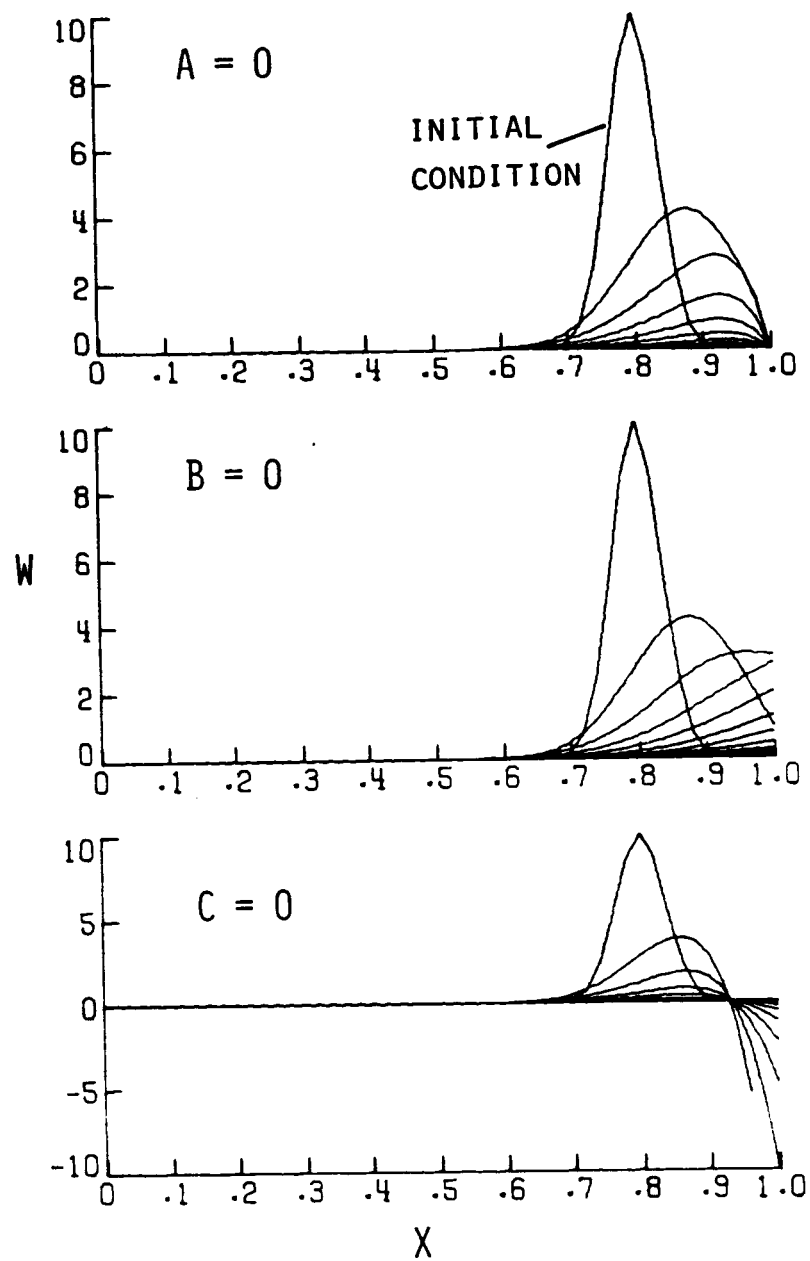
(R = 25, J = 50, Δt = .0025; plotted every 30Δt).

Fig. 5. w vs. x for correct steady state outflow conditions.

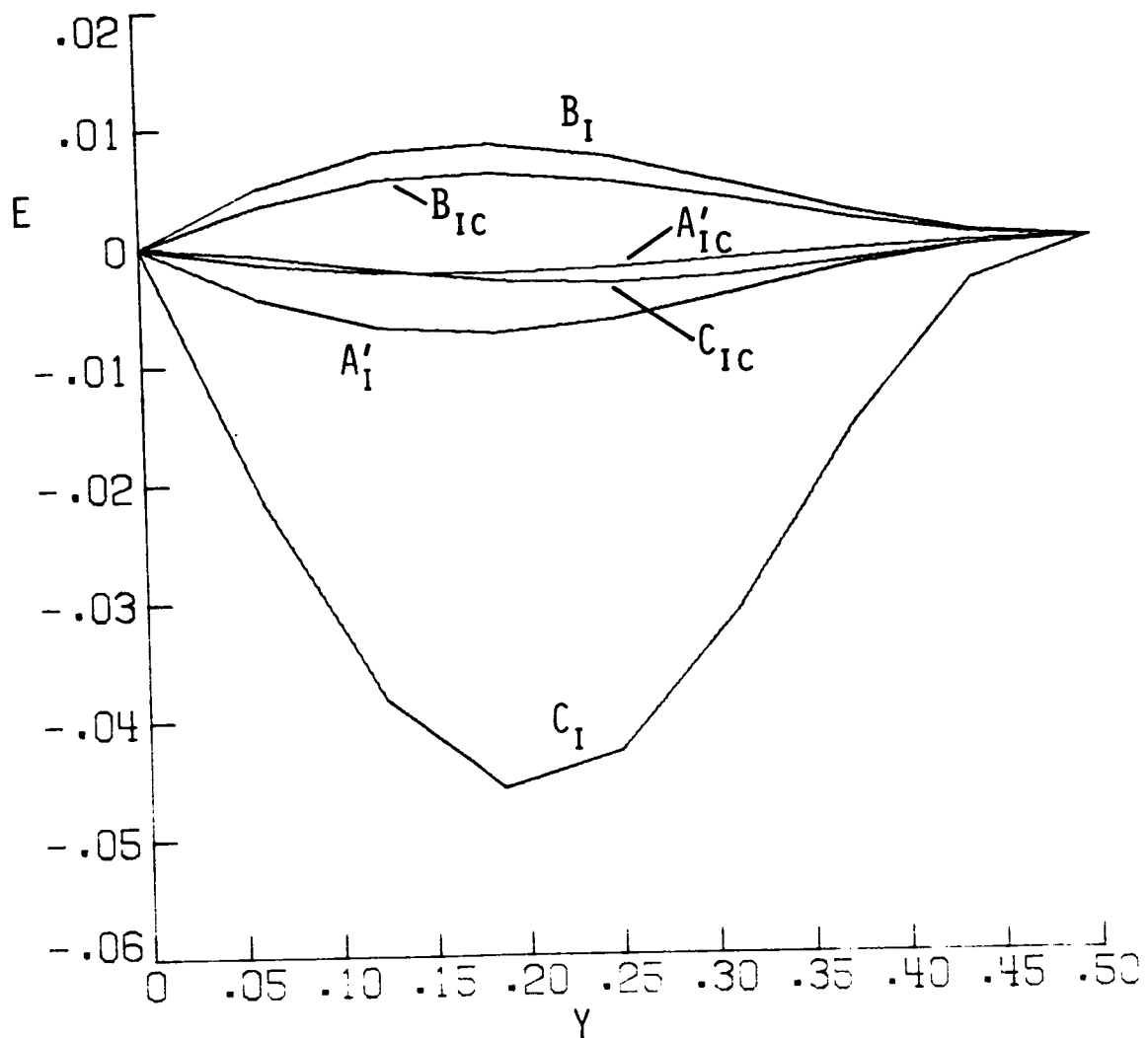(R = 25, J = 50, Δt = .0025; plotted every 30Δt).

Fig. 6. Error in the steady state streamfunction at $x = 1/2$. $[E = (\Psi - \Psi_E)/\bar{\Psi}_E]$

($R = 20$, $\Delta x = \Delta y = h = 1/16$; $I = $ "incorrect" calculation,
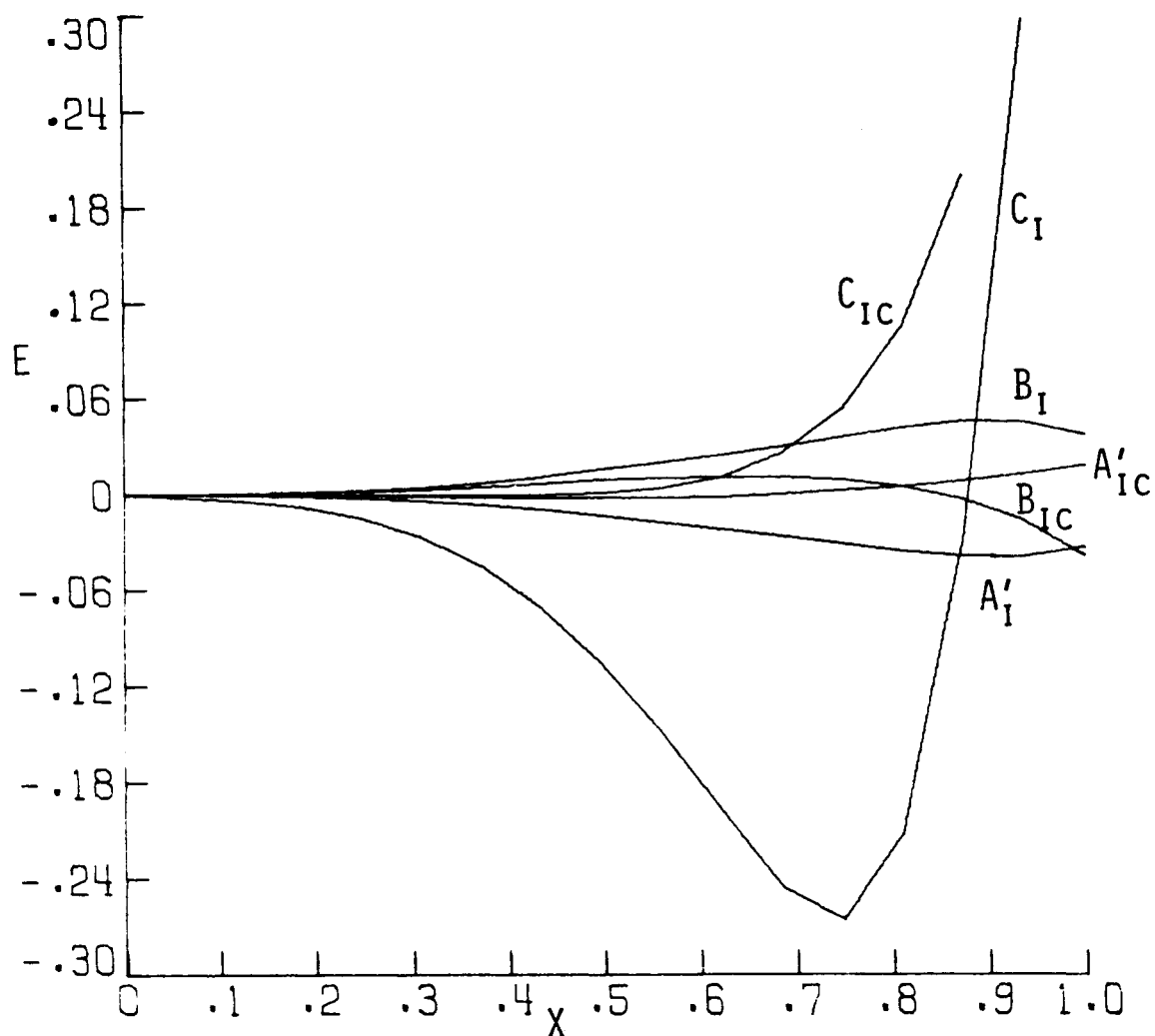
$IC = $ "incorrect - correct" calculation).

Fig. 7. Error in the steady state vorticity at $y = 1/4$. $[E = (\zeta - \zeta_E)/\bar{\zeta}_E]$ ($R = 20$, $\Delta x = \Delta y = h = 1/16$; I = "incorrect" calculation, IC = "incorrect - correct" calculation).
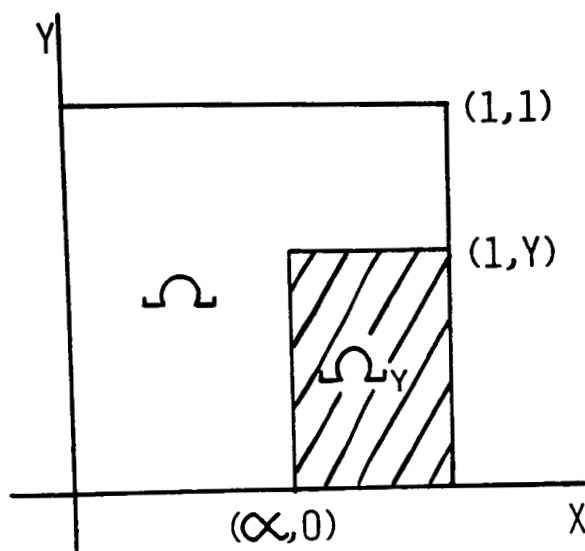
Fig. 8.   The regions Ω and Ω_y.